ORIGINAL PAPER

Inverse finite element characterization of the human thigh soft tissue in the seated position

Sheng Chen[1] · Justin Scott[1] · Tamara Reid Bush[1] · Sara Roccabianca[1]

Abstract
Pressure ulcers are localized damage to the skin and underlying tissues caused by sitting or lying in one position for a long time. Stresses within the soft tissue of the thigh and buttocks area play a crucial role in the initiating mechanism of these wounds. Therefore, it is crucial to develop reliable finite element models to evaluate the stresses caused by physiological loadings. In this study, we compared how the choice of material model and modeling area dimension affect prediction accuracy of a model of the thigh. We showed that the first-order Ogden and Fung orthotropic material models could approximate the mechanical behavior of soft tissue significantly better than neo-Hookean and Mooney–Rivlin. We also showed that, significant error results from using a semi-3D model versus a 3D model. We then developed full 3D models for 20 participants employing Ogden and Fung material models and compared the estimated material parameters between different sexes and locations along the thigh. We showed that males tissues are less deformable overall when compared to females and the material parameters are highly dependent on location, with tissues getting softer moving distally for both men and women.

Keywords Soft tissue · Nonlinear mechanical behavior · Finite element · Optimization · Pressure ulcer

1 Introduction

Pressure ulcers (PUs), also known as pressure sores, are localized damage to the skin and underlying tissues, usually occurring over a bony prominence and caused by sitting or lying in one position for a long time. PUs are detrimental to the well-being of people who lose their mobility either permanently or temporarily and are associated with high morbidity and mortality (Gefen 2008). Each year in the US an estimated 2.5 million people develop PUs (Reddy et al. 2006). In the year 2013, almost 30,000 deaths were caused by complications associated with this condition, globally (GBD 2013 Mortality and Causes of Death Collaborators 2015). Furthermore, PUs take a long time to heal, ranging from several weeks to several months and the healing is often not complete, leading to a high reoccurrence rate (Nordqvist 2017).

Several hypotheses have been made on how PUs develop, including cellular death due to mechanical distortion (Ryan 1990), tissue decay due to reduced interstitial flow and lymphatic drainage (Reddy et al. 1981) or reduced blood perfusion (Herrman et al. 1999), and localized ischemia (Bouten et al. 2003). Although the initiating mechanism of PUs is still unclear, it is commonly accepted that internal normal and shear stresses, due to the presence of unrelieved external loads, play a central role in the formation and development of these wounds (Manorama et al. 2010). Therefore, it is crucial to evaluate the internal stresses caused by the physiological loading conditions of sitting or lying down to assess the risk of tissue injury. Due to the nonlinear and anisotropic nature of soft biological tissue and the complicated anatomy of different tissue groups (i.e., muscle, bone, fat) it is nearly impossible to estimate subdermal stress/strain fields just from superficial skin pressure measurement.

Finite element (FE) models have the ability of accurately represent the anatomical structure of the leg and buttocks area and to estimate the localized stress/strain field within highly deformable media. For this reason, FE models have proved to be powerful tools to investigate soft tissue response to external loadings. Due to the limited computational power, early FE models used simplified

✉ Sara Roccabianca
  roccabis@egr.msu.edu

[1] Department of Mechanical Engineering, Michigan State University, 428 S. Shaw Lane Room 2463, East Lansing, MI 48824, USA

geometries (Chow and Odell 1978; Dabnichki et al. 1994; Ragan et al. 2002). To further diminish the computational load, some studies developed 3D models initially and later simplified them to 2D models assuming axisymmetry (Chow and Odell 1978; Ragan et al. 2002), while other studies developed 2D models from the start by assuming plane strain or plane stress conditions (Dabnichki et al. 1994; Brosh and Arcan 2000). More recently, researchers created anatomically accurate 3D models for the thigh and buttock areas by employing medical images (Makhsous et al. 2007; Al-Dirini et al. 2016). Yet, semi-3D models (i.e., a 3D model that has one dimension significantly smaller than the others) and 2D models still remain popular among researchers (Linder-Ganz et al. 2007; Linder-Ganz and Gefen 2007; Rohan et al. 2015; Shoham et al. 2015). Due to the nearly incompressible nature of soft biological tissues, however, significant deformations will occur transversely to the loading direction, especially in large deformations, which has been shown before through MRI images during sitting (Sonenblum and Sprigle 2013; Sonenblum et al. 2015; Al-Dirini et al. 2015), which are harder to appreciate in 2D and semi-3D models. In this study, we compared 3D and semi-3D models in the following two ways: (1) by comparing the best-fit material parameters estimated in 3D versus semi-3D models, employing the same in vivo dataset; and (2) by comparing the displacement field predicted by 3D versus semi-3D models, employing the same material parameters.

Finally, which material model one chooses to describe the highly nonlinear mechanical behavior of soft biological tissues also plays an important role in developing an accurate FE model. Early FE studies employed linear elastic material models (Chow and Odell 1978; Ragan et al. 2002). In more recent years, four hyperelastic models can commonly be found in the literature, neo-Hookean (Linder-Ganz et al. 2007; Linder-Ganz and Gefen 2007), Mooney–Rivlin (Makhsous et al. 2007; Verver et al. 2004), the first-order Ogden (Oomens et al. 2003; Al-Dirini et al. 2016), and Fung-type exponential (Holzapfel et al. 2004; Sun and Sacks 2005). There are, however, no guidelines for the choice of material model due to the paucity of in vivo experimental data. A recent paper from this group presented, for the first time, a large data set that describes the in vivo large deformations behavior of the leg and buttock areas, for multiple locations on multiple participants (Sadler et al. 2018). This gives us the opportunity to fill the need for a study that compares the accuracy of different material models (e.g., neo-Hookean, Mooney–Rivlin, Ogden, and Fung) in the description of the mechanical behavior of soft tissues of the thigh and buttocks. To achieve this, we developed an optimization process that can minimize the difference between experimentally measured and FE simulated force–deflection curves. We then compared best-fit material parameters to detect differences in soft tissue mechanical properties between sexes and regions.

2 Materials and methods

2.1 Mechanical testing

We recorded force–deflection data sets from the leg for 20 individuals: 10 males (average age: 20.6, average weight: 76.2 kg, average height: 170.4 cm) and 10 females (average age: 20.9, average weight: 66.4 kg, average height: 162.8 cm), following a previously published protocol (Sadler et al. 2018). Briefly, we first recorded standard anthropometric measurements, such as height, weight, seated height, buttocks width, and leg dimensions for each participant. Each participant was seated on the ischial tuberosity so that the soft tissue of the thigh was unloaded and undeformed. Then, we used a custom made hand-held compression device to gather force–deflection data on the proximal, middle, and distal locations on the posterior side of the thigh. Load was applied until a biological barrier was reached.

2.2 Geometry generation

We recorded the specific geometry for one representative participant (female) employing the following protocol. The participant was seated on the ischial tuberosity so that the thigh was not deformed and the knee was flexed at 90°. We used a Sense^{TM} V2 3D scanner to record the CAD model of the thigh (Fig. 1b). A femur geometry obtained from GrabCAD (Alexis 2016) was placed within the model of the thigh, and we used anthropometric measurements of the participant and CT images of thigh cross sections from the literature (Strandberg et al. 2010) to ensure the correct size and the accurate position of the femur.

The geometry of the remaining 19 participants was obtained by employing a scaling technique starting from the geometry of the one representative participant (Brandon et al. 2017). Specifically, the singular thigh CAD model developed was scaled to that of another participant by matching two key participant-specific measurements collected at the time of mechanical testing, namely the length from hip joint to knee joint and the circumference of the middle thigh. All participants weight and height fell into the US mid-size male and female groups previously published (Gordon et al. 1989). This enabled us to use a constant diameter for the femur within the same sex group, while the diameter of the femur of male participants was increased by 4.8% with respect to that of female participants (Looker et al. 2001).

Fig. 1 a Schematic of the seating positioning for a participant during 3D scanning. **b** Thigh CAD model obtained from 3D scanning of the thigh of a representative participant. **c** Representative 3D FE model. **d** Dimensions and positioning of testing areas for the 3D FE model, on top, and the semi-3D FE model, on the bottom. From left to right, proximal, middle, and distal thigh testing locations are shown in red. **e** Flow chart of the material parameter optimization protocol
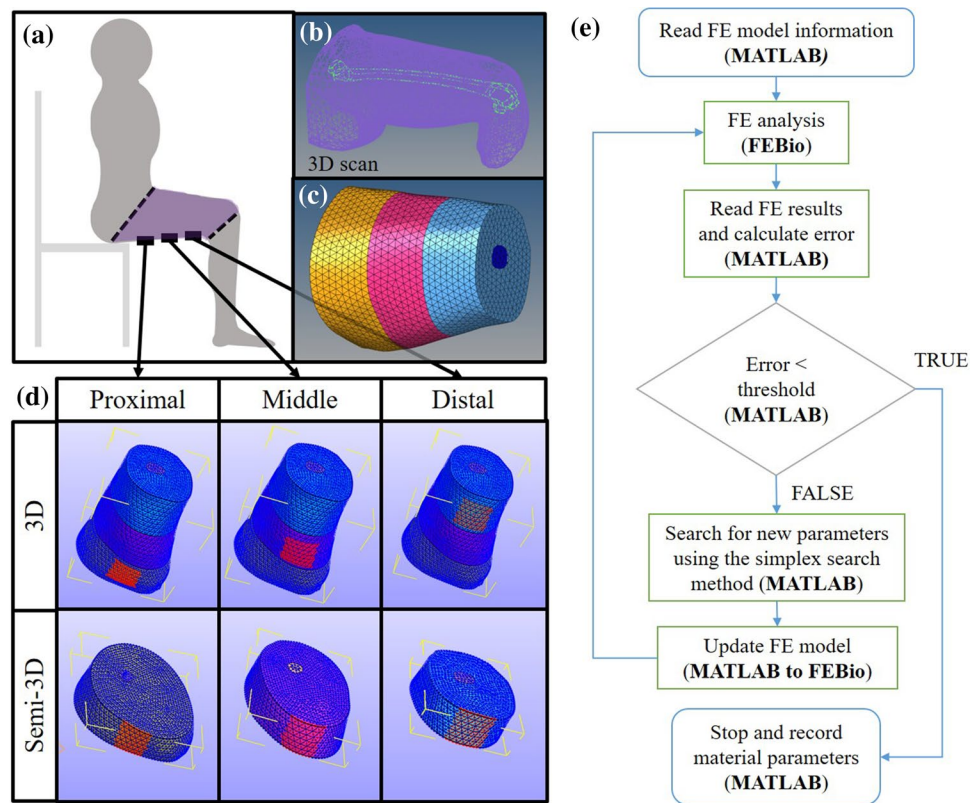
2.3 Finite element model

2.3.1 Mesh generation

Each CAD model was cut along two transverse planes, one passing through the joint between buttock and thigh and another passing through the joint between thigh and knee (Fig. 1c). Then, the model was meshed (HyperMesh ver.13.0) using 10 node tetrahedral elements of size 10 mm. The FE models have an average of 32,062 elements and 47,518 nodes. A mesh sensitivity study was conducted using the representative participant's model with elements of size 10 mm (i.e., 27,724 elements, 41,227 nodes), elements of size 7.5 mm (i.e., 54,568 elements, 79,830 nodes), and elements of size 5 mm (i.e., 141,083 elements, 203,742 nodes). We compared the normalized root mean square deviations [NRMSDs, Eq. (9)] between force–deflection curves of the FE model with 10 mm-sized elements and the FE model with 7.5 mm and 5 mm-sized elements, at each tested location. All NRMSDs are below 2.2%. This confirms that mesh convergence was achieved using elements of size 10 mm. The soft tissues in the model were then divided into three locations, corresponding to the three testing sites (see Sect. 2.1). The same homogenous material model but different material parameters described the lumped

mechanical properties of soft tissues (i.e., skin, fat, and muscle) at each location, and the femur was modeled as a rigid body.

2.3.2 3D model

Three 50 mm × 50 mm areas were identified at the proximal, middle, and distal locations on the posterior side of the thigh (see Fig. 1d, top row), each corresponding to a location tested during the in vivo experiment. Boundary conditions were applied to the femur (i.e., constrained against displacement and rotation in any direction), to the two cut planes at proximal and distal thigh (i.e., nodes were constrained against displacements along the femur longitudinal direction), and to the three testing areas (i.e., nodes were restricted to move only in the direction perpendicular to the seat surface). Additionally, participant-specific compression forces at each location, as recorded in vivo, were applied to one testing area at a time. Compression forces were applied in 20 evenly spaced steps from zero to the maximum value recorded in the experiment, and the nodal displacements of the compressed area at each step were recorded and averaged. Simulated force–deflection curves were then compared to the experimental data to estimate the best-fit material parameters.

2.3.3 Semi-3D model

Additionally, we developed three semi-3D FE models of one representative participant. We cut the thigh CAD model at the proximal, middle, and distal tested areas, respectively, using two transverse planes placed at 50 mm from one other. These three 50 mm long (in the femur longitudinal direction) CAD models were then meshed using the same element type and element size as the 3D FE model described above (Fig. 1d bottom row). The boundary conditions applied to the femur, cut planes, and tested areas, the load application procedure, and the material parameter estimation were the same as discussed above for the full 3D model. We then compared the best-fit material parameters of 3D and semi-3D FE models that described the same set of experimental data, as well as the simulated force–deflection data of 3D and semi-3D FE model estimated employing the same set of material parameters.

2.4 Material models and parameter optimization

2.4.1 Neo-Hookean model

The strain energy function for the neo-Hookean model (Rivlin 1948) was defined as

$$\Psi^{nH} = c_1^{nH}\left(I_C - 3\right) + \frac{1}{2}K^{nH}(\ln J)^2, \tag{1}$$

where c_1^{nH} is a material parameter with the dimension of a stress, $I_C = \mathrm{tr}(\mathbf{C})$ is the first invariant of the right Cauchy-Green strain tensor, $\mathbf{C} = \mathbf{F}^T\mathbf{F}$, $\mathbf{F}$ is the deformation gradient, and $J = \det(\mathbf{F})$ is the third invariant of $\mathbf{F}$. In the principal reference system, one could write $\mathbf{F} = \mathrm{diag}\left[\lambda_1, \lambda_2, \lambda_3\right]$, where λ_1, λ_2, and λ_3 represent the stretches in the principal directions. The coefficient K^{nH} represents the bulk modulus-like penalty parameter, which is defined as $K^{nH} = \frac{2c_1^{nH}}{(1-2\upsilon)}$, where υ represents the Poisson's ratio. In all the material descriptions presented in this work we considered the Poisson's ratio to be $\upsilon = 0.485$ (Makhsous et al. 2007) to ensure a nearly incompressible material description.

2.4.2 Mooney–Rivlin model

The strain energy function for the Mooney–Rivlin model (Rivlin 1949) was defined as

$$\Psi^{MR} = c_1^{MR}\left(I_C - 3\right) + c_2^{MR}\left(II_C - 3\right) + \frac{1}{2}K^{MR}(\ln J)^2, \tag{2}$$

where c_1^{MR} and c_2^{MR} are material parameters with the dimension of a stress, I_C is the first invariant of $\mathbf{C}$ and J is the third invariant of $\mathbf{F}$, as defined above, and $II_C = \frac{1}{2}\left[(\mathrm{tr}(\mathbf{C}))^2 - \mathrm{tr}\left(\mathbf{C}^2\right)\right]$ is the second invariant of the tensor $\mathbf{C}$. The bulk modulus-like penalty parameter K^{MR} is defined as $K^{MR} = \frac{2(c_1^{MR}+c_2^{MR})}{(1-2\upsilon)}$.

2.4.3 First-order Ogden model

The strain energy function for the first-order Ogden model (Ogden 1972) was defined as

$$\Psi^{Ogd} = \frac{\mu^{Ogd}}{\alpha^{Ogd}}\left(\lambda_1^{\alpha^{Ogd}} + \lambda_2^{\alpha^{Ogd}} + \lambda_3^{\alpha^{Ogd}} - 3\right) + \frac{1}{2}K^{Ogd}(\ln J)^2, \tag{3}$$

where μ^{Ogd} and α^{Ogd} are material parameters with the dimension of a stress and dimensionless, respectively, J is the third invariant of $\mathbf{F}$, and λ_1, λ_2, and λ_3 represent the stretches in the principal directions, as defined above. The bulk modulus-like penalty parameter K^{Ogd}, is defined as $K^{Ogd} = \frac{\mu^{Ogd}\alpha^{Ogd}}{2(1-2\upsilon)}$. We defined also the parameter low strain stiffness as

$$E^{Ogd} = \frac{3}{2}\mu^{Ogd}\alpha^{Ogd}, \tag{4}$$

which corresponds to the Young's modulus in the infinitesimal elasticity theory, i.e., represents the slope of the stress–strain curve under uniaxial loading when the material undergoes small deformation.

2.4.4 Fung orthotropic model

With the assumption of isotropic symmetry, the strain energy function of the Fung orthotropic model (Ateshian and Costa 2009) was defined as

$$\Psi^F = \frac{1}{2}c^F\left(e^{\tilde{Q}} - 1\right) + \frac{1}{2}K^F(\ln J)^2, \tag{5}$$

where c^F is a material parameter with the dimension of a stress, J is the third invariant of $\mathbf{F}$, $K^F = \frac{E^F}{3(1-2\upsilon)}$ is the bulk modulus-like penalty parameter, and E^F represents the low strain stiffness parameter, i.e., the Young's modulus in the infinitesimal elasticity theory. Finally, we defined the exponential parameter $\tilde{Q}$ as

$$\tilde{Q} = \gamma^F(\mathbf{I} : \mathbf{E})^2 + \gamma^F\frac{(1-2\nu)}{\nu}\mathbf{I} : \mathbf{E}^2, \tag{6}$$

where $\mathbf{E} = \frac{1}{2}(\mathbf{C} - \mathbf{I})$ is the Green strain tensor, $\mathbf{I}$ is the identity tensor, and the dimensionless material parameter γ^F is defined as

$$\gamma^F = \frac{E^F\nu}{c^F(1+\nu)(1-2\nu)}. \tag{7}$$

2.4.5 Material parameter optimization protocol

Material parameters at proximal, middle, and distal thigh locations were optimized employing the simplex search method implemented in MATLAB (i.e., function *fminsearch*). The FE simulation in each optimization iteration was performed employing the FEBio 2.4.1 implicit solver. The flowchart of the optimization process is shown in Fig. 1e. The goal of the optimization process was to minimize the difference between the FE simulated force–deflection curves and the experimental data at each location. The objective function to be minimized was

$$e = \mathrm{NRMSD_{prx}} + \mathrm{NRMSD_{mid}} + \mathrm{NRMSD_{dis}}, \qquad (8)$$

where $\mathrm{NRMSD_{prx}}$, $\mathrm{NRMSD_{mid}}$, and $\mathrm{NRMSD_{dis}}$ are NRMSD estimated at each location α as

$$\mathrm{NRMSD}_\alpha = \frac{\sqrt{\frac{\sum_{i=1}^{n}\left(d_\alpha^{\mathrm{FE}}-d_\alpha^{\mathrm{EXP}}\right)_i^2}{n}}}{\left(d_\alpha^{\mathrm{EXP}}\right)_{\max}} \qquad (9)$$

where n is the number of loading steps (i.e., $n = 20$), d_α^{FE} and d_α^{EXP} are the deflection values for the α location from the FE simulation and experimental measurement, respectively, and $\left(d_\alpha^{\mathrm{EXP}}\right)_{\max}$ represents the maximum experimental values of deflection for each location α (i.e., the deflection measure for the maximum load). The initial-guess material parameters for each material model were obtained from the literature, as shown in Table 1, and all material parameter values were constraint to be positive.

2.5 Statistical analysis

After the best-fit material parameters of all 20 participants were obtained, statistical analysis was carried out to determine the influence of sex and location on material parameters. Student's *t* test was utilized to determine influence of sex on material parameters at each thigh location, while one-way repeated measures ANOVA, followed by Holm–Sidak post hoc test, was utilized to determine the influence of location on material parameters within each sex group.

3 Results

3.1 Effects of the choice of material model and of modeling region dimension

All results in this Section have been evaluated considering the geometry and mechanical properties collected experimentally for one representative participant.

3.1.1 Effect of the choice of material model

Material model effects were investigated using a 3D FE model. Figure 2 shows experimentally measured (symbols) and numerically calculated (lines) compression force–deflection curves for each thigh location and for each material model considered. All sections of Fig. 2a–d show the same three sets of experimental data collected in vivo. Each section of Fig. 2 also shows the numerical results for a 3D FE model, each of these models has the same geometry, and the soft tissue is described employing one of the four material models (Fig. 2a–d, respectively). The numerical results shown have been obtained employing the optimized material parameters, and the results are presented for each testing location, namely proximal (solid), middle (dashed), and distal thigh (dotted). Values of best-fit material parameters for each material model and each location are also reported in Table 2. The NRMSD, Eq. (9), between the 3D FE simulation and the experimental data was calculated for each tested location and for each material model adopted, in addition to the total NRMSD, Eq. (8). The neo-Hookean model had the largest total NRMSD (35%), followed by the Mooney–Rivlin model (26%), the Fung model (18%), and finally the first-order Ogden model (8%). In the analysis of the datasets of the overall 20 participants we employed Fung orthotropic and the Ogden material models.

Table 1 Initial-guess material parameters for each material model

Material model	Material parameter	Initial-guess parameter value	Reference
Neo-Hookean	c_1^{nH} (KPa)	8.50	Linder-Ganz et al. (2007)
Mooney–Rivlin	c_1^{MR} (KPa)	1.65	Verver et al. (2004)
	c_2^{MR} (KPa)	3.35	
Ogden	μ^{Ogd} (KPa)	3	Oomens et al. (2003)
	α^{Ogd}	30	
Fung orthotropic	E^{F} (KPa)	10	Pilot investigation of current study
	c^{F} (KPa)	10	

Fig. 2 Compression force–deflection curves from experimental measures (symbols) and model predictions (lines) for each location and each material model considered. **a–d** The same experimental data are shown in every section, representing the mechanical behavior for representative participant F6 at the proximal (triangles), middle (circles), and distal (asterisks) locations. Also shown are the model predictions after parameter optimization for each location, namely proximal (solid line), middle (dashed line), and distal (dotted line). The models considered are **a** neo-Hookean, **b** Mooney–Rivlin, **c** Ogden, and **d** Fung orthotropic
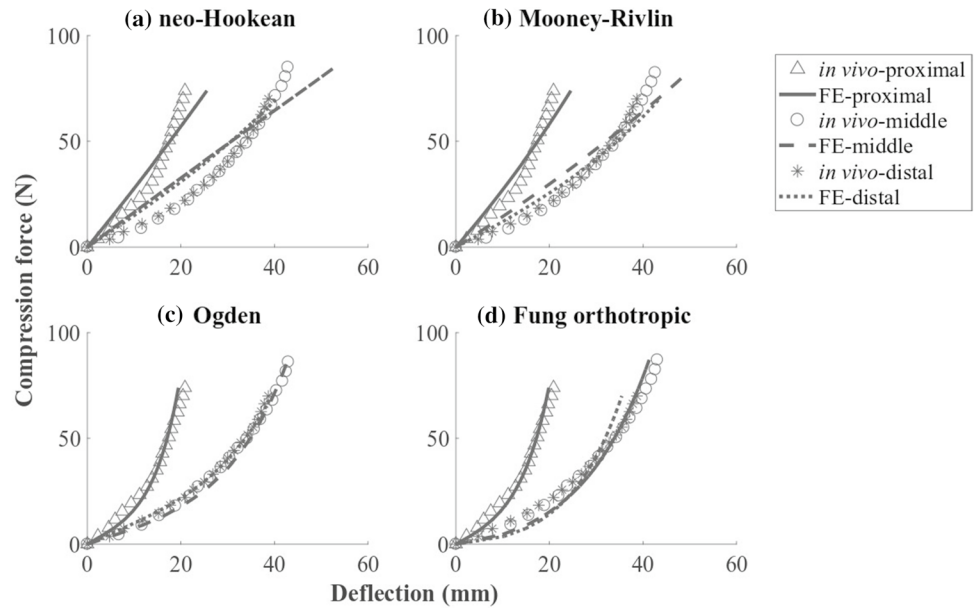

Table 2 Best-fit material parameters of 3D and semi-3D FE models at proximal, middle, and distal thigh location employing each material model (i.e., neo-Hookean, Money–Rivlin, Ogden, Fung orthotropic)

Material model	Material parameter	Proximal thigh			Middle thigh			Distal thigh		
		3D	Semi-3D	%	3D	Semi-3D	%	3D	Semi-3D	%
Neo-Hookean	c_1^{nH} (KPa)	8.50	11.90	40.0	3.12	5.74	84.0	3.02	3.61	19.5
Mooney–Rivlin	c_1^{MR} (KPa)	2.18	2.22	1.8	1.49	1.74	16.8	1.73	1.84	6.4
	c_2^{MR} (KPa)	6.00	9.69	61.5	1.11	3.92	253.2	0.62	1.84	196.8
Ogden	μ^{Ogd} (KPa)	0.49	2.30	369.4	0.49	2.38	385.7	1.70	3.43	101.8
	α^{Ogd}	35.78	12.97	− 63.8	11.85	6.00	− 49.4	5.38	3.50	− 34.9
Fung orthotropic	E^F (KPa)	25.30	18.25	− 27.9	3.00	5.98	99.3	2.70	3.22	19.3
	c^F (KPa)	3.20	0.95	− 70.3	16.70	13.41	− 19.7	23.30	16.31	− 30.0

Experimental data collected for representative subject F6 have been used to inform the 3D and semi-3D FE model (Fig. 1). The percentage difference of best-fit material parameters between the two types of model at each thigh location are shown in the column titled as "%" (Note: positive values indicate semi-3D model have higher parameter values, and negative values indicate 3D model have higher parameter values)

3.1.2 Effect of the choice of modeling region dimension

First, we compared best-fit material parameters optimized for 3D and semi-3D FE models for the three thigh regions, employing the same experimental data set. Percentage differences between the semi-3D and 3D models are shown in Table 2. The largest difference occurred at the middle thigh location for each material model: 84% for neo-Hookean, 253.2% for Mooney–Rivlin, 385.7% for Ogden, and 99.3% for Fung.

We then compared force–deflection mechanical behavior of the 3D and semi-3D FE models employing the best-fit material parameters evaluated for the 3D FE model shown in Fig. 3. The figure shows deflection differences between the semi-3D FE model and 3D FE model (i.e., $d^{semi \text{-} 3D} - d^{3D}$)

for each material model at each location (Fig. 3a–c, respectively).

The NRMSD between the semi-3D and the 3D FE model for each material model and each location were also calculated. A total value of NRMSD is reported here, estimated as the sum of the values at each location. The Mooney–Rivlin material model showed the largest total NRMSD (81%), followed by the neo-Hookean (64%), Ogden (38%), and Fung (29%). It is important to notice that the effect of the modeling region dimension choice (semi-3D vs. 3D) affects the predicted behavior more dramatically than the choice of material model, based on the value of total NRMSD.
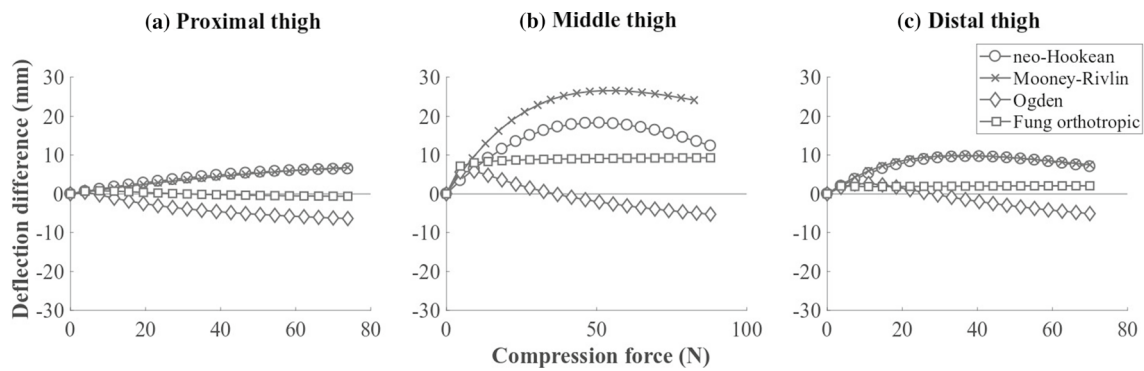
Fig. 3 Mechanical behavior comparison between 3D and semi-3D FE thigh models of participant F6 at **a** proximal thigh, **b** middle thigh, and **c** distal thigh. Horizontal axis represents forces applied to the soft tissue of thigh at each loading step, while the vertical axis represents deflection difference between semi-3D FE model and 3D FE model at each loading step, i.e., $d^{\text{semi-3D}} - d^{\text{3D}}$

3.2 Effect of sex and location

Best-fit material parameters for Ogden and Fung models were obtained for all 20 participants, employing 3D geometries scaled to match the anatomical measures of each participant. Figure 4 shows box plots for the material parameters for both models, grouped by sex (i.e., male and female) and location (i.e., proximal, middle, and distal thigh). Specifically, Fig. 4 shows the parameters μ^{Ogd}, α^{Ogd}, and E^{Ogd} for the Ogden model on the left, where E^{Ogd} is calculated employing Eq. (4). The parameters c^{F}, γ^{F}, and E^{F} for the Fung orthotropic model are shown on the right, where γ^{F} is calculated employing Eq. (7).

3.2.1 Effect of sex

The material parameters for each model were compared between males and females at each location. The results of the statistical analysis are presented in Table 3. For the Ogden model, Student's t test found that males have a significantly higher value of μ^{Ogd} at the proximal thigh location ($p < 0.05$), as well as a higher value of E^{Ogd} at the proximal and middle thigh locations ($p < 0.05$ for both locations) when compared to females. For the Fung orthotropic model, males have a higher value of E^{F} at the middle thigh location ($p < 0.05$), and a higher value of γ^{F} at the proximal thigh location ($p < 0.05$).

3.2.2 Effect of location

Since we detected multiple differences in material parameters between male and female participants, we analyzed the effect of location on the material parameters within the same sex. One-way repeated measures ANOVA found that location had a significant effect on (1) α^{Ogd} and E^{Ogd} for the

Ogden model ($p < 0.001$ for both parameters and for both male and female group) and (2) all material parameters E^{F}, c^{F}, and γ^{F} for the Fung orthotropic model ($p < 0.001$ for both male and female group for all parameters).

To better understand which location comparisons contribute to the differences in the material parameters, we carried out a Holm–Sidak post hoc pairwise test for the following locations: proximal versus middle, proximal versus distal, and middle versus distal. The results of the statistical analysis are presented in Table 4.

4 Discussion

Nonlinearity is a unique characteristic of soft biological tissues, failing to include that within models could significantly affect the accuracy of the predictions. However, to be able to capture nonlinear behavior in large deformations, one needs to have access to experimental data that (1) record both forces and deformations simultaneously and (2) expand over an appropriate loading range. In other words, there is a need for data from a mechanical test that captures the in vivo mechanical behavior of soft tissues under large deformations, in an appropriate full-body configuration (i.e., seated vs. laying down). Such data sets have not been available until recently (Sadler et al. 2018). Previously published data still made an effort to describe the nonlinearity of the thigh and buttocks soft tissues. For example, some studies obtain material parameters from the literature and later validate the FE model by reporting the error between the FE simulation and the experimental data (Verver et al. 2004; Linder-Ganz et al. 2007; Makhsous et al. 2007). Other studies perform an optimization to estimate the best-fit material parameters that minimize the error between the FE simulation and the experimental data in one specific configuration (Ragan et al. 2002; Al-Dirini et al. 2016). The experimental data available
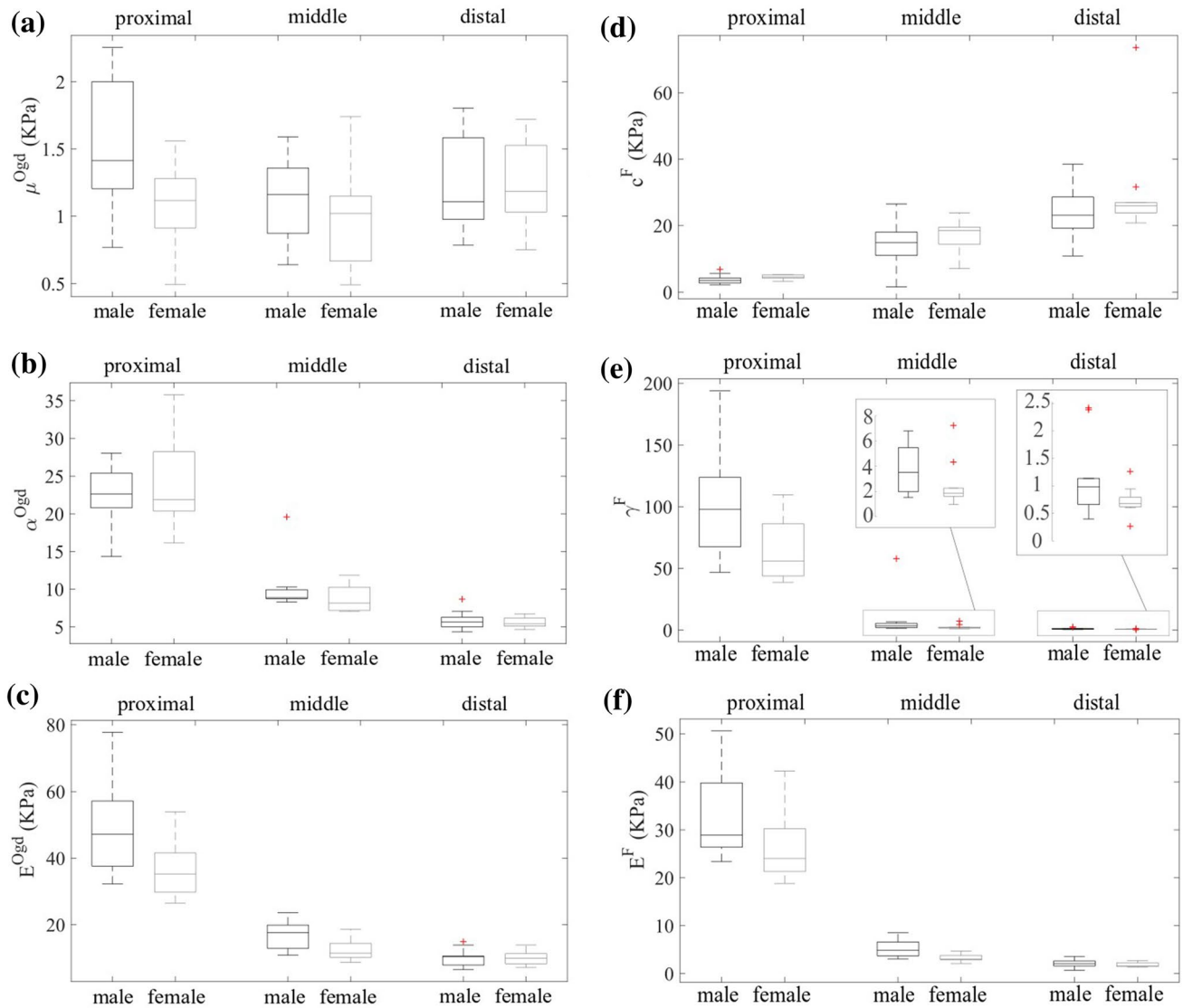
Fig. 4 Best-fit Ogden model and Fung orthotropic model parameters, i.e., **a** μ^{Ogd}, **b** α^{Ogd}, **c** E^{Ogd}, **d** c^{F}, **e** γ^{F}, and **f** E^{F} for 20 tested participants, at proximal, middle, and distal thigh locations, respectively. Parameter values are grouped based on location (marked at the top of each plot) and sex (marked at the bottom of each plot). The central mark within the box indicates the group median, and the bottom and top edges of the box indicate the 25th and 75th percentiles, respectively. The whiskers extend to the most extreme data points, not considering outliers, and the outliers are plotted individually using the '+' symbol

for both approaches are, however, limited and describe the deformations corresponding to one loading configuration (i.e., weight-bearing configuration in upright sitting position). Due to the nonlinear behavior of soft tissues, we propose that to have access to data in only two configurations, namely an unloaded position and a loaded seated position, is not sufficient to describe accurately the mechanical behavior of the tissues. This is a pressing issue, especially when determining the stress distributions within the tissue that cannot be directly experimentally validated.

The optimization procedure in this study compares deflection estimated by FE simulation to deflection from a unique experimental dataset collected in vivo for a value of loading that gradually increases from 0 to a maximum load (Sadler et al. 2018). Because of the continuous nature of the experimental dataset, this work has the capability of accurately describing the mechanical behavior of the thigh soft tissues for a large range of loading configurations. For this reason, we have the opportunity to compare the accuracy of four different materials models in describing the behavior of soft tissues, for one representative subject. We show that 3D FE models employing neo-Hookean and Mooney–Rivlin material models (i.e., NRMSD = 35% and 26%, respectively) describe the soft tissue's mechanical behavior of the thigh

Table 3 p values of Student's t test comparing sex difference at different thigh locations

	Male versus female		
	Proximal thigh	Middle thigh	Distal thigh
μ^{Ogd}	*0.038*	0.429	0.865
α^{Ogd}	0.682	0.235	0.547
E^{Ogd}	*0.023*	*0.021*	0.846
c^{F}	0.170	0.502	0.223
γ^{F}	*0.035*	0.252	0.105
E^{F}	0.101	*0.004*	0.297

Material parameters tested are from Ogden and Fung material models. The italic values highlight the statistical significance, i.e., $p < 0.05$

less accurately than Fung orthotropic and the first-order Ogden material models (i.e., NRMSD = 18% and 8%, respectively). We observe that neo-Hookean and Mooney–Rivlin material model underestimate deformations at the low force level and overestimate deformations at the high force level (Fig. 2a, b). In other words, neo-Hookean and Mooney–Rivlin material models do not capture the nonlinearity of the in vivo data. In comparison, Fung orthotropic model overestimates deformations at the low force level and underestimates deformations at the high force level (Fig. 2d). In other words, Fung orthotropic material model overestimates the nonlinearity of the in vivo data of the representative subject. Finally, the first-order Ogden material model offers the lowest error (Fig. 2c). The strain energy function's formulation of each material model could justify the behavior observed. Being a polynomial function with exponents values that are real and specific for each dataset, the first-order Ogden material model can describe a broad range of nonlinear mechanical behavior. While neo-Hookean and Mooney–Rivlin have integer and fixed exponents value, therefore, the nonlinear mechanical behavior they can describe are constrained. Similarly, the mechanical behaviors that Fung orthotropic material model can accurately describe are constrained by the exponential function. After examining the force–deflection behavior characteristics of data from the remaining 20

subjects, we determine that neo-Hookean and Mooney–Rivlin material models are not suitable to describe the highly nonlinear in vivo data in this study. Therefore, Fung and the first-order Ogden model are employed for the remaining 20 FE models. It is important to notice that neo-Hookean and Mooney–Rivlin material models are still commonly used in soft tissue modeling (Manafi-Khanian et al. 2016; Silva et al. 2018), our results, however, suggest that these material models should be used with care, along with proper experimental data, parameter optimization process, and detailed microstructural information (Myers et al. 2015).

In this study, we also quantify the differences between 3D and semi-3D FE models, in two ways: (1) the material parameter differences when fitting the same set of experimental data and (2) the force–deflection mechanical behavior differences when employing the same material parameters. Regarding the first approach, semi-3D models can overestimate some mechanical parameters and underestimate others when compared to 3D models, as shown in Table 2. In terms of low strain stiffness, semi-3D model depicts experimental data in a stiffer fashion when compared to the 3D model [low strain stiffness defined as $E^{\mathrm{nH}} = 6c_1^{\mathrm{nH}}$, $E^{\mathrm{MR}} = 6\left(c_1^{\mathrm{MR}} + c_2^{\mathrm{MR}}\right)$, $E^{\mathrm{Ogd}} = \frac{3}{2}\mu^{\mathrm{Ogd}}\alpha^{\mathrm{Ogd}}$, and E^{F} as given in Eq. (7)]. The second approach results are shown in Fig. 3, where a positive deflection difference value indicates that semi-3D models show a more compliant behavior when compared to the 3D FE model, while a negative value indicates a less compliant behavior. When neo-Hookean or Mooney–Rivlin constitutive laws are employed, the deflection differences are positive for all values of load at all locations, suggesting that semi-3D models behave in a more compliant way when compared to the 3D FE model. The same behavior is observed for the Fung model at the middle and distal locations. In this case, the use of material parameters estimated for a 3D model to perform a semi-3D analysis will lead to underestimating the load needed to cause a certain displacement and ultimately to underestimating the stress distribution within the thigh. On the other hand, when the Ogden model is employed in all locations and the Fung orthotropic model is employed at the proximal location, the deflection difference

Table 4 p values of Holm–Sidak post hoc pairwise tests comparing model parameter difference between different thigh locations

	Male			Female		
	Prx versus Mid	Prx versus Dis	Mid versus Dis	Prx versus Mid	Prx versus Dis	Mid versus Dis
α^{Ogd}	*< 0.001*	*<0.001*	*<0.001*	*<0.001*	*<0.001*	*<0.001*
E^{Ogd}	*< 0.001*	*<0.001*	*<0.001*	*<0.001*	*<0.001*	0.052
c^{F}	*< 0.001*	*<0.001*	**0.020**	*<0.001*	*0.001*	**0.050**
γ^{F}	*< 0.001*	*<0.001*	0.186	*<0.001*	*<0.001*	**0.017**
E^{F}	*< 0.001*	*<0.001*	*<0.001*	*<0.001*	*<0.001*	*0.001*

Material parameters tested are from Ogden and Fung material models. The bold and italic values highlight the statistical significance, a bold values corresponds to statistical significance ($p < 0.05$), and a italic values corresponds to strong statistical significance ($p < 0.001$)

have positive values for small loads and negative values for large loads. This suggests that, when using parameters that have been optimized for a 3D model to perform a semi-3D FE analysis, one will overestimate the values of loads needed to apply a large deflection. This will likely lead to overestimating the stress state within the tissue, specifically for the seated condition.

We propose that the effect due to a choice of modeling region dimension (i.e., semi-3D vs. 3D) can largely affect mechanical prediction. The best-fit material parameters can be significantly different between a semi-3D model when compared to fully 3D models when optimized using the same experimental dataset. Furthermore, when using material parameters optimized for a 3D model to perform a semi-3D analysis, the error in the prediction can be as high as 44.56%. While we do not think that the specific conclusions based on a single-subject study are generalizable, due to the complexity of subject-specific soft tissue geometries and boundary conditions, we want to highlight that significant differences between semi 3D model and full 3D model exist and need to be taken into account when comparing results from different studies. Furthermore, even within the single-subject study, the difference between semi-3D and 3D model are inhomogeneous and unpredictable. For instance, the semi-3D model can both underestimate and overestimate the values of E^F based on location, as shown in Table 2, and it can both overestimate and underestimate predicted displacement based on material model, as shown in Fig. 3. These results suggest that, when describing the same in vivo mechanical behavior, material parameters obtained from one modeling condition can be significantly different than parameters obtained from a different modeling condition; so comparison between them might be misleading. These results also suggest that one needs to be careful when using material parameters that have been estimated in a specific modeling condition to perform an analysis in a different modeling condition.

After showing that Ogden and Fung orthotropic are the more accurate models among the four considered here for the representative participant, the best-fit material parameters are evaluated for the remaining 19 participants. A statistical analysis has been carried out to highlight potential differences in mechanical properties between sexes and between locations. Male participants are found to have consistently higher low strain tissue stiffness than female participants, regardless of material model, at the proximal thigh (E^{Ogd} and E^F) and middle thigh (E^F) location (Table 3). This might be caused by the different compositions of cross sections between men and women, specifically women are found to have a higher fat content when compared to men (Kanehisa et al. 1994).

Also, we detect a high location-dependence of material parameters across material models. Specifically, the proximal location shows to be significantly stiffer (higher values of E^{Ogd} and E^F) when compared to the middle and distal location for both men and women (Table 4). Furthermore, the middle location proves to be significantly stiffer when compared to the distal location for both men and women (Table 4). This suggests that the thigh tissue increases its compliance moving distally from the buttocks. This result confirms what have been reported in Mergl et al. (2004), where soft tissues in the thigh–buttock area are modeled using a linear elastic isotropic material, with four different regions described by four different Young's modulus values, respectively. The material parameters estimated in that study show a similar stiffening trend across thigh locations as what we have reported here. The sex and location differences on low strain stiffness found in the current study employing Ogden and Fung orthotropic constitutive law agree with a previous study from this same group that uses a simplified uniaxial compression model employing Mooney–Rivlin constitutive law to describe the same experimental dataset (Sadler et al. 2018). The sex and location influences on the material parameters shown above indicate the importance of individual and location specific in vivo measurement of biological soft tissue in FE modeling. Furthermore, the present results show that this modeling approach has the capability of detecting mechanical differences between groups, in a consistent way, independent of the nonlinear model of choice (e.g., Fung or Ogden model).

The current study has some limitations. First, the thigh geometry generation lacks subject-specific data. While we have collected the specific surface geometry for the representative subject, the geometry of the femur and the determination of femur relative position within the thigh are based on the literature sources. Furthermore, the FE models of the remaining 19 subjects also lack surface geometry details; however, we ensure that the femur size and its relative position are within anatomically reasonable ranges, and the hip-joint lengths and the middle thigh circumferences of the other 19 subjects are matched to subject-specific data. Second, the thigh soft tissues are modeled by the use of a bulk material; thus, the material parameters are evaluated based on different locations rather than soft tissue types. Having access to a more precise anatomy of the soft tissues within the thigh, possibly through medical imaging, will give us the capability of estimating mechanical properties correlated to specific tissues rather than locations. It has been shown by previous MRI study that the muscle strain is more sensitive to changes in seat support surface and load distribution than strain in subcutaneous fat (Al-Dirini et al. 2017), which could be an important characteristic to validate an anatomically accurate FE model and further increase its predicting capability. This will be the focus of future investigations. Third, the bulk properties of soft tissues in the present study are modeled using isotropic material models, although

the mechanical properties of soft tissues (e.g., muscle and skin) have been known to be anisotropic. Due to the lack of multi-axial in vivo experimental data and to the choice of modeling the soft tissues as a bulk material, however, using isotropic material models is a reasonable option (Manafi-Khanian et al. 2016; Silva et al. 2018). Fourth, the optimization process in this study used the simplex search algorithm (*fminsearch* function in MATLAB). The use of this algorithm is motivated by the fact that it is a derivative-free method. Algorithms like trust-region would require gradient information of the objective function; however, the objective function in our study has no analytic expression and performs like a black box: Inputs are the material parameters and outputs are the NRMSDs between the FE simulation and experimental data. Due to the lack of analytic expressions, the convexity of the objective function cannot be confirmed, which opens the possibility of the optimized material parameters to be local minima instead of global minima.

The current study is a comprehensive investigation of finite element modeling regarding nonlinear mechanical behavior of human thigh soft tissue. We proposed an optimization process that addressed the nonlinear characteristic of in vivo force–deflection data, which has been neglected in the literature. For the first time, we compared the ability of four widely used material models in describing soft tissue nonlinear behavior. Also, for the first time in the literature, we investigated the effect of the choice of modeling region dimension (3D vs. semi 3D). We also reported material parameter range for Ogden and Fung orthotropic models based on in vivo force–deflection data for 20 participants. This study provided deep insights and reliable data for researchers interested in nonlinear mechanical behavior of human soft tissues.

Compliance with ethical standards

Conflict of interest The authors declare that they have no conflict of interest.

Reference

Al-Dirini RMA, Reed MP, Thewlis D (2015) Deformation of the gluteal soft tissues during sitting. Clin Biomech 30:662–668. https://doi.org/10.1016/j.clinbiomech.2015.05.008

Al-Dirini RMA, Reed MP, Hu J, Thewlis D (2016) Development and validation of a high anatomical fidelity FE model for the buttock and thigh of a seated individual. Ann Biomed Eng 44:2805–2816. https://doi.org/10.1007/s10439-016-1560-3

Al-Dirini RMA, Nisyrios J, Reed MP, Thewlis D (2017) Quantifying the in vivo quasi-static response to loading of sub-dermal tissues in the human buttock using magnetic resonance imaging. Clin Biomech 50:70–77. https://doi.org/10.1016/j.clinbiomech.2017.09.017

Alexis B (2016) James (human body for scale) | 3D CAD model library | GrabCAD. In: GRABCAD. https://grabcad.com/library/james-human-body-for-scale-1. Accessed 10 Apr 2018

Ateshian GA, Costa KD (2009) A frame-invariant formulation of Fung elasticity. J Biomech 42:781–785. https://doi.org/10.1016/j.jbiomech.2009.01.015

Bouten CV, Oomens CW, Baaijens FP, Bader DL (2003) The etiology of pressure ulcers: skin deep or muscle bound? Arch Phys Med Rehabil 84:616–619. https://doi.org/10.1053/apmr.2003.50038

Brandon SCE, Smith CR, Thelen DG (2017) Simulation of soft tissue loading from observed movement dynamics. In: Müller B, Wolf SI, Brueggemann G-P et al (eds) Handbook of human motion. Springer, Cham, pp 1–34

Brosh T, Arcan M (2000) Modeling the body/chair interaction–an integrative experimental–numerical approach. Clin Biomech 15:217–219

Chow WW, Odell EI (1978) Deformations and stresses in soft body tissues of a sitting person. J Biomech Eng 100:79–87. https://doi.org/10.1115/1.3426196

Dabnichki PA, Crocombe AD, Hughes SC (1994) Deformation and stress analysis of supported buttock contact. Proc Inst Mech Eng H 208:9–17. https://doi.org/10.1177/095441199420800102

GBD 2013 Mortality and Causes of Death Collaborators (2015) Global, regional, and national age-sex specific all-cause and cause-specific mortality for 240 causes of death, 1990–2013: a systematic analysis for the Global Burden of Disease Study 2013. Lancet 385:117–171. https://doi.org/10.1016/S0140-6736(14)61682-2

Gefen A (2008) How much time does it take to get a pressure ulcer? Integrated evidence from human, animal, and in vitro studies. Ostomy Wound Manag 54(26–8):30–35

Gordon CC, Churchill T, Clauser CE et al (1989) Anthropometric survey of U.S. Army personnel: summary statistics, interim report for 1988. Anthropology Research Project Inc., Yellow Springs

Herrman EC, Knapp CF, Donofrio JC, Salcido R (1999) Skin perfusion responses to surface pressure-induced ischemia: implication for the developing pressure ulcer. J Rehabil Res Dev Wash 36:109–120

Holzapfel GA, Gasser TC, Ogden RW (2004) Comparison of a Multilayer structural model for arterial walls with a Fung-type model, and issues of material stability. J Biomech Eng 126:264–275. https://doi.org/10.1115/1.1695572

Kanehisa H, Ikegawa S, Fukunaga T (1994) Comparison of muscle cross-sectional area and strength between untrained women and men. Eur J Appl Physiol 68:148–154. https://doi.org/10.1007/BF00244028

Linder-Ganz E, Gefen A (2007) The effects of pressure and shear on capillary closure in the microstructure of skeletal muscles. Ann Biomed Eng 35:2095–2107. https://doi.org/10.1007/s10439-007-9384-9

Linder-Ganz E, Shabshin N, Itzchak Y, Gefen A (2007) Assessment of mechanical conditions in sub-dermal tissues during sitting: a combined experimental-MRI and finite element approach. J Biomech 40:1443–1454. https://doi.org/10.1016/j.jbiomech.2006.06.020

Looker AC, Beck TJ, Orwoll ES (2001) Does body size account for gender differences in femur bone density and geometry? J Bone Miner Res 16:1291–1299. https://doi.org/10.1359/jbmr.2001.16.7.1291

Makhsous M, Lim D, Hendrix R et al (2007) Finite element analysis for evaluation of pressure ulcer on the buttock: development and validation. IEEE Trans Neural Syst Rehabil Eng 15:517–525. https://doi.org/10.1109/TNSRE.2007.906967

Manafi-Khanian B, Arendt-Nielsen L, Graven-Nielsen T (2016) An MRI-based leg model used to simulate biomechanical phenomena during cuff algometry: a finite element study. Med Biol Eng Comput 54:315–324. https://doi.org/10.1007/s11517-015-1291-x

Manorama AA, Baek S, Vorro J et al (2010) Blood perfusion and transcutaneous oxygen level characterizations in human skin with changes in normal and shear loads—implications for pressure ulcer formation. Clin Biomech 25:823–828. https://doi.org/10.1016/j.clinbiomech.2010.06.003

Mergl C, Anton T, Madrid-Dusik R et al (2004) Development of a 3D finite element model of thigh and pelvis. SAE International, Warrendale, PA. https://doi.org/10.4271/2004-01-2132

Myers KM, Hendon CP, Gan Y et al (2015) A continuous fiber distribution material model for human cervical tissue. J Biomech 48:1533–1540. https://doi.org/10.1016/j.jbiomech.2015.02.060

Nordqvist C (2017) Bed sores or pressure sores: what you need to know. In: Medical news today. https://www.medicalnewstoday.com/articles/173972.php. Accessed 10 Apr 2018

Ogden RW (1972) Large deformation isotropic elasticity—on the correlation of theory and experiment for incompressible rubberlike solids. Proc R Soc Lond A 326:565–584. https://doi.org/10.1098/rspa.1972.0026

Oomens CWJ, Bressers OFJT, Bosboom EMH et al (2003) Can loaded interface characteristics influence strain distributions in muscle adjacent to bony prominences? Comput Methods Biomech Biomed Eng 6:171–180. https://doi.org/10.1080/1025584031000121034

Ragan R, Kernozek TW, Bidar M, Matheson JW (2002) Seat-interface pressures on various thicknesses of foam wheelchair cushions: a finite modeling approach. Arch Phys Med Rehabil 83:872–875. https://doi.org/10.1053/apmr.2002.32677

Reddy NP, Cochran GVB, Krouskop TA (1981) Interstitial fluid flow as a factor in decubitus ulcer formation. J Biomech 14:879–881. https://doi.org/10.1016/0021-9290(81)90015-4

Reddy M, Gill SS, Rochon PA (2006) Preventing pressure ulcers: a systematic review. JAMA 296:974–984. https://doi.org/10.1001/jama.296.8.974

Rivlin RS (1948) Large elastic deformations of isotropic materials. I. Fundamental concepts. Philos Trans R Soc Lond A 240:459–490. https://doi.org/10.1098/rsta.1948.0002

Rivlin RS (1949) Large elastic deformations of isotropic materials VI. Further results in the theory of torsion, shear and flexure. Philos Trans R Soc Lond A 242:173–195. https://doi.org/10.1098/rsta.1949.0009

Rohan P-Y, Badel P, Lun B et al (2015) Prediction of the biomechanical effects of compression therapy on deep veins using finite element modelling. Ann Biomed Eng 43:314–324. https://doi.org/10.1007/s10439-014-1121-6

Ryan TJ (1990) Cellular responses to tissue distortion. In: Bader DL (ed) Pressure sores - clinical practice and scientific approach. Palgrave, London, pp 141–152. https://doi.org/10.1007/978-1-349-10128-3_11

Sadler Z, Scott J, Drost J et al (2018) Initial estimation of the in vivo material properties of the seated human buttocks and thighs. Int J Non-Linear Mech. https://doi.org/10.1016/j.ijnonlinmec.2018.09.007

Shoham N, Levy A, Kopplin K, Gefen A (2015) Contoured foam cushions cannot provide long-term protection against pressure-ulcers for individuals with a spinal cord injury: modeling studies. Adv Skin Wound Care 28:303. https://doi.org/10.1097/01.ASW.0000465300.99194.27

Silva E, Parente M, Brandão S et al (2018) Characterizing the biomechanical properties of the pubovisceralis muscle using a genetic algorithm and the finite element method. J Biomech Eng 141:011009–011009–011009–011011. https://doi.org/10.1115/1.4041524

Sonenblum SE, Sprigle SH (2013) Response of the authors to: comments on "validation of an accelerometer-based method to measure the use of manual wheelchairs" by Sonenblum et al. Med Eng Phys 2012; 34(6):781–6. Med Eng Phys 35:556–557. https://doi.org/10.1016/j.medengphy.2013.01.005

Sonenblum SE, Sprigle SH, Cathcart JM, Winder RJ (2015) 3D anatomy and deformation of the seated buttocks. J Tissue Viability 24:51–61. https://doi.org/10.1016/j.jtv.2015.03.003

Strandberg S, Wretling M-L, Wredmark T, Shalabi A (2010) Reliability of computed tomography measurements in assessment of thigh muscle cross-sectional area and attenuation. BMC Med Imaging 10:18. https://doi.org/10.1186/1471-2342-10-18

Sun W, Sacks MS (2005) Finite element implementation of a generalized Fung-elastic constitutive model for planar soft tissues. Biomech Model Mechanobiol 4:190–199. https://doi.org/10.1007/s10237-005-0075-x

Ververs MM, van Hoof J, Oomens CWJ et al (2004) A finite element model of the human buttocks for prediction of seat pressure distributions. Comput Methods Biomech Biomed Eng 7:193–203. https://doi.org/10.1080/10255840410001727832